

RSC Advances



This is an *Accepted Manuscript*, which has been through the Royal Society of Chemistry peer review process and has been accepted for publication.

Accepted Manuscripts are published online shortly after acceptance, before technical editing, formatting and proof reading. Using this free service, authors can make their results available to the community, in citable form, before we publish the edited article. This *Accepted Manuscript* will be replaced by the edited, formatted and paginated article as soon as this is available.

You can find more information about *Accepted Manuscripts* in the [Information for Authors](#).

Please note that technical editing may introduce minor changes to the text and/or graphics, which may alter content. The journal's standard [Terms & Conditions](#) and the [Ethical guidelines](#) still apply. In no event shall the Royal Society of Chemistry be held responsible for any errors or omissions in this *Accepted Manuscript* or any consequences arising from the use of any information it contains.

Dynamic Behavior of Curved Double-wall Carbon Nanotubes with Rotating Inner Tube

Kun Cai^a, Haifang Cai^a, Hang Yin^a, Qing H. Qin^{b*}

^a College of Water Resources and Architectural Engineering, Northwest A&F University, Yangling 712100, China

^b Research School of Engineering, the Australian National University, Acton, ACT 2601, Australia

*corresponding author's email: Qinghua.qin@anu.edu.au

Kun Cai's email address: caikun1978@163.com

ABSTRACT

It is noted that an oscillator from a curved double-walled nanotubes can provide a local stronger periodic adjustable magnetic field than that from a straight double-walled carbon nanotubes when the inner tube loses electric neutrality at ends. Therefore, it is interesting to study the damped rotational and oscillatory behavior of curved double-wall carbon nanotubes (DWCNTs) through a molecular dynamics (MD) simulation approach. As the outer tube is curved, intuitively, the intertube friction becomes stronger. Hence, the rotational and oscillatory characteristics of a single-wall carbon nanotube (SWCNT) within a curved outer tube might be obviously different from those of SWCNTs within straight DWCNTs. To investigate the effects of curvature on dynamic behavior, a straight (9, 9)/(14, 14) DWCNTs is geometrically mapped into three curved bitube systems with different curvatures. In the microcanonical NVE ensemble, the inner tube with initial high speed rotation has damped rotation and oscillation along the curved axis of the outer tube. Energy transfer between two curved tubes is faster than that between two straight tubes. Further, the oscillation of the inner tube is disordered when the curvature is relatively high. The rotational frequency of an inner tube in a curved outer tube decreases more quickly than that in a straight outer tube. Effects of temperature on dynamic behavior of curved double-walled nanotubes are also investigated through a numerical example.

Keywords: Double-wall carbon nanotube, curved carbon nanotube, damped rotation, molecular dynamics

1. Introduction

In recent decades, the excellent mechanical, electrical, and thermal properties of CNTs have attracted much attention from engineers and scientists considering potential applications in micro-electromechanical systems (MEMS) and nano-electromechanical systems (NEMS)^{1,2} and strain sensors^{3,4}. Among these remarkable properties, the low interaction between adjacent walls of multiwalled carbon nanotubes (MWCNTs) has been studied experimentally^{5,6,7} with regard to the sliding of neighboring shells in MWCNTs. This phenomenon has inspired a series of studies for CNT oscillators and resonators.

Following the work of Cumings and Zettl⁵ on pulled core tubes formed by opening one end

of capped MWCNTs, Zheng and Jiang⁸ proposed a continuum mechanics-based static model of a gigahertz MWCNT oscillator with both ends of the outer shells opened. As a supplement, further detailed theoretical calculation⁹ of the excess van der Waals energy due to the extrusion and corresponding force was proposed. The results showed that the oscillating frequency could reach several gigahertz, and that finding inspired a series of studies focusing on this distinctive behavior. The dynamic stability of the oscillators was first considered by Leogas et al.¹⁰, who presented molecular dynamics (MD) simulations to investigate oscillation using many combinations of CNT diameter and chirality. They concluded that a stable oscillation of the CNT system could be captured only when the radius difference between adjacent walls of the system was around 3.4 Å. Further study was undertaken to understand the influence of such factors as CNT length and configuration on the pattern of energy dissipation in nano-oscillators. For example, Zhao et al.¹¹ found that a steep rocking motion of the walls in short DWCNT oscillators (with length greater than 3 nm) appeared when the inner wall was pulled about one-third out of the outer wall. Rivera et al.^{12,13} simulated the oscillation of incommensurate DWCNTs with lengths between 12.21 and 98.24 nm. Their results implied that the inner tube had damped oscillatory behavior at gigahertz frequencies, and its corresponding amplitude showed linear dependence on the tube length. Guo et al.¹⁴ found that the energy dissipation of an incommensurate DWCNT oscillator was smaller than that in a commensurate oscillator, although the results differed somewhat from the self-oscillation model proposed by Cai et al.¹⁵. It should also be mentioned that oscillators with controllable amplitude¹⁶ and frequency¹⁷ have been developed recently.

In all the simulation studies mentioned above, the oscillation models were assumed to be straight MWCNTs. However, experimental images show that the tubes are generally curved. Besides, comparing with the oscillator from a straight DWCNT, an oscillator from curved double-walled nanotubes can provide a local stronger periodic adjustable magnetic field when the inner tube loses electric neutrality at ends. Hence, a curved oscillator can be adopted in NEMS for signal transmission. In recent years, some researchers have begun to focus on the mechanical behavior of curved CNTs. For example, Üstünel et al.¹⁸ modeled a curved CNT or nanowire as a clamped-clamped elastic beam and studied the structural vibration. Mayoof and Hawwa¹⁹ studied the chaotic behavior of a curved single-walled CNT with a sinusoidal curvature. Xia and Wang²⁰ compared the vibration characteristics of curved and straight CNTs in a conveying fluid. Ouakad and Younis²¹ studied the vibration behavior of CNT resonators under electric excitation. Ghavanloo et al.²² investigated the vibration behavior of a SWCNT conveying fluid and embedded the system into a viscoelastic medium. Artan and Tepe²³ studied nonlocal effects of curved CNTs. Eichler et al.²⁴ presented a detection method to demonstrate the symmetry breaking of a curved CNT with low-frequency motion. The above studies were based on continuum mechanics theory. In 2013, Fakhraabadi et al.²⁵ used MD simulation to investigate the deformations and pull-in charges of SWCNT beams with different geometries. To the authors' knowledge, no work has focused on the dynamics behavior of a curved DWCNT. In our present work, we use the MD technique to investigate the damped rotational and oscillatory behavior of a curved DWCNT with a high speed rotating inner tube.

2. Methods

2.1 Geometrical mapping of a shell

In the present MD simulations, a straight DWCNT with the chirality (9, 9)/(14, 14) (Fig 1a, b) is firstly considered. The lengths of the inner and outer tubes are 10.10 nm and 7.98 nm, respectively, and the pre-pullout inner tube stays aligned with outer tube at one end of the DWCNT (Fig 1c). To obtain curved DWCNTs with selected degrees of curvature, the geometric mapping approach for a shell is employed. Typically, an arbitrary point $P(x, y, z)$ on the I-I cross section of a shell is mapped with point $P^*((x^*, y^*, z^*))$ in the same coordinate system as in Fig 2, and the relations between the two coordinates can be given by the following formulations:

$$\begin{cases} x^* = x + (\rho_0 - x) \cdot (1 - \cos \phi_1), \\ y^* = y, \\ z^* = (\rho_0 - x) \cdot \sin \phi_1. \end{cases} \quad (1)$$

where $\rho_0 = \frac{L}{\phi_{\max}}$ is the radius of the curved axis (τ), $\phi_1 = \frac{z}{\rho_0}$ is the angle between the normal direction of the I-I section and the z axis, L is the length of the shell, and ϕ_{\max} is the curvature angle of the shell, which is taken as the values of 0° , 5° , 15° , and 25° for the outer tube in curved DWCNTs. Except for the protrudes part that remains straight, the axis of the inner tube has the same curvature as that of the outer tube. Fig. 1(c) shows the four simulation models after the geometrical mapping described above.

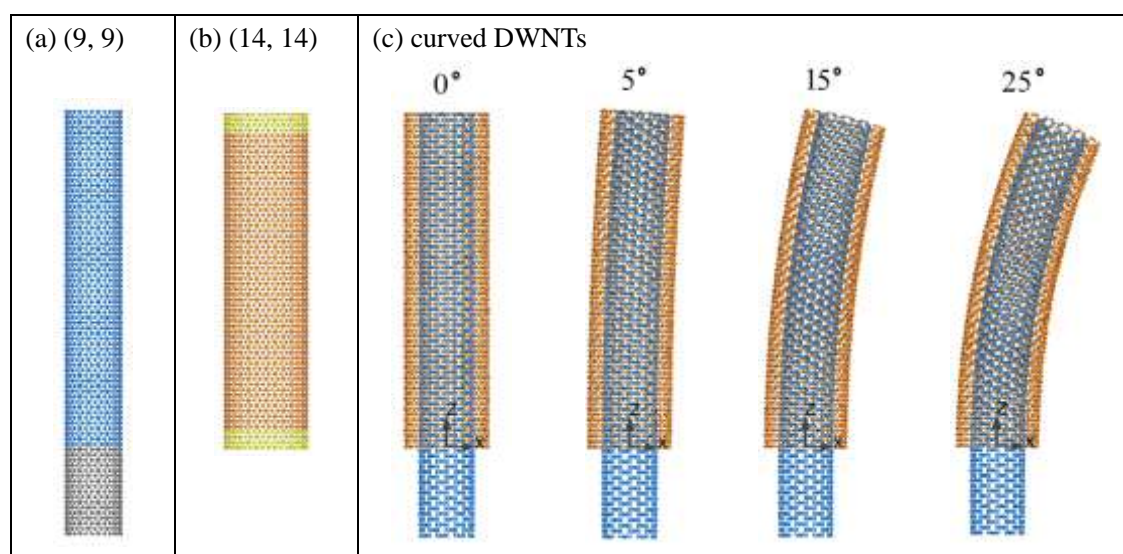


Fig.1 Simulation models of DWCNTs (a) inner tube (9, 9) with length of 10.10nm (81 layers), (b) outer tube with length of 7.98nm (64 layers), (c) curved DWNTs from the inner tube in (a) and outer tube in (b) (the difference in radii is ~ 0.335 nm), and the protruded part (grey atoms in (a)) of the inner tube remains straight before the end of relaxation. The central angles are 0° (straight), 5° , 15° , and 25° , and four layers (yellow atoms in (b)) near each end of the outer tube are fixed in the simulation.

2.2 Simulation parameters

In the present simulations, the force field of the adaptive intermolecular reactive empirical bond order (AIREBO) potential²⁶ is used, which is well known for the description of both covalent

bonds between carbon atoms and the long-range van der Waals interactions. It should be mentioned that the AIREBO potential²⁶ has been widely used in nano-engineering^{14, 15, 26, 27} due to its relatively high accuracy in describing the interactions between C-C or C-H bonds and long range vdW force between two atoms/molecules. The AIREBO potential combines REBO potential energy, L-J potential energy and torsional energy. Especially, the torsion of bonds is measured in AIREBO potential which is important in the current simulation for description of large deformation of shell. It can reflect chemical reactions (bond broken or generation). However, bond broken happens only when the deformation of a bond is large enough. Based on this understanding, the effect of chemical reaction on the result can be ignored in the present study. Therefore, the parameters are sufficient to express the bending of outer tube and associated C-C bonds.

Commonly, curved tubes after geometrical mapping have high potential because no relaxation occurs. Hence, at the beginning of simulation, 500ps of relaxation is carried out while the inner tube is rotating with 125GHz (or 8ps of period) at the canonical NVT ensemble ($T=100, 300$ or 500 K). During relaxation, the inner tube is fixed along the curved axis (τ).

In this study, both in NVE and NVT ensembles, the damping motion of the inner tube are simulated. For example, after relaxation, we change the NVT ensemble into an NVE ensemble and release the inner tube to begin rotating and vibrating freely along the curved axis (τ). To investigate the temperature effect on the damping motion of the inner tube, we also simulate the system in the canonical NVT ensemble with different environmental temperature after relaxation. 3000,000 steps of iteration are simulated with the time step of 1 femtosecond.

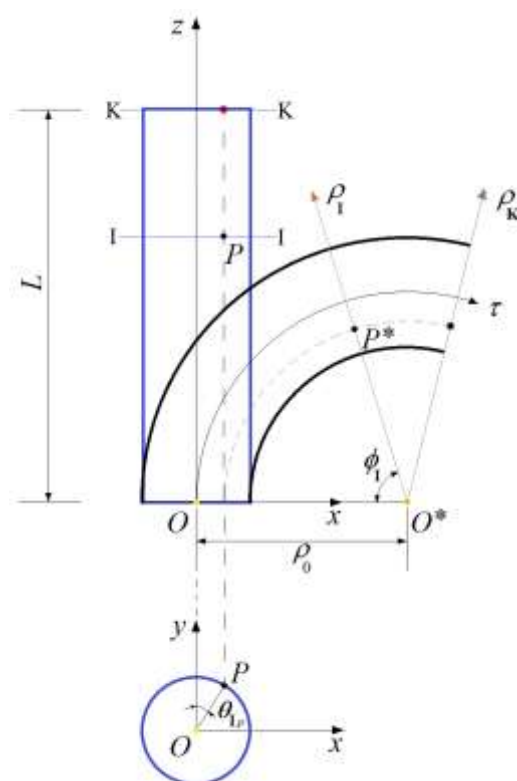


Fig. 2 Geometrical mapping scheme of a shell with constant curvature

3. Discussion and conclusions

3.1 Temperature history of bitube systems in NVE ensemble

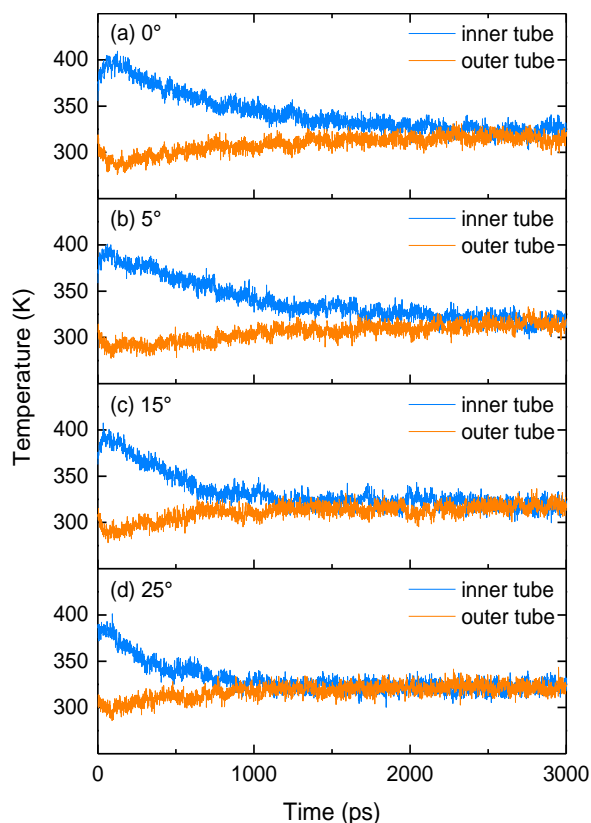


Fig 3 Temperature histories of inner and outer tubes in different curved DWCNTs.

From Fig 3 it can be seen that in each case, the temperature of the inner tube drops with the increase in the temperature of the outer tube within the first 100 ps. Thus the energy transfer from the inner to the outer tube obviously occurs during this period. But in the subsequent simulation period, a contrary phenomenon appears, i.e., the temperature of the inner tube increases with the decrease of that of the outer tube. The major reason is that the inner tube begins oscillating along the curved axis (τ) (Fig 2). In the system, the temperatures of inner and outer tubes tend to be identical. Table 1 lists the average temperatures of the inner and outer tubes in different curved DWCNTs during the 2501st ps to 3000th ps.

Considering the temperatures listed in Table 1 as stable values of the tubes, the time when the stable state approaches is different for different DWCNTs. For example, the temperatures of tubes in the straight (0°) DWCNTs approach stable values after about 2500 ps. For 5° curved DWCNTs, the comparative time is about 2200 ps. For 15° and 25° curved DWCNTs, the comparative times are about 1200 ps and 800 ps, respectively. It is concluded that the temperature converges more quickly to the stable value for DWCNTs with greater curvature.

Table 1 Average temperature of inner and outer tubes in different curved DWCNTs during [2501, 3000] ps

Curvature	0°	5°	15°	25°
Inner tube (K)	323.396	317.438	318.475	322.967

Outer tube (K)	316.166	314.616	317.903	321.469
----------------	---------	---------	---------	---------

3.2 Oscillatory behavior of inner tubes in curved outer tubes

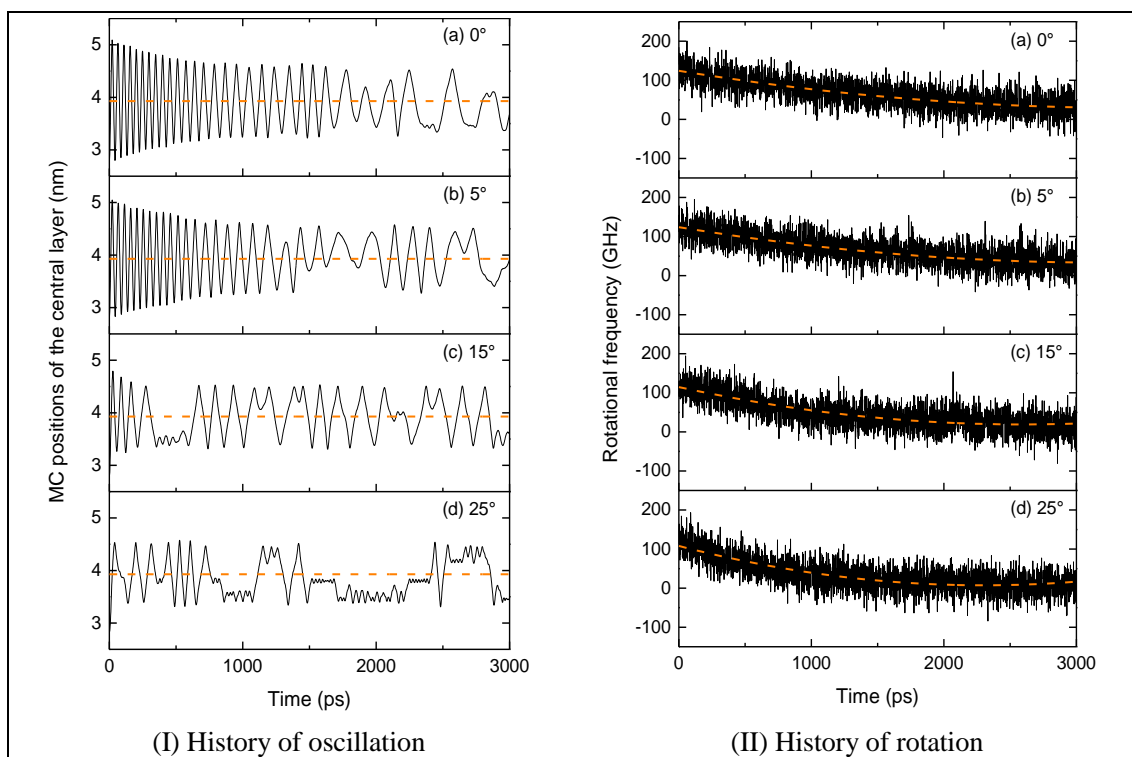


Fig 4 Damping motions of the inner tube in a NVE ensemble. (I) Oscillatory behavior of inner tube along curved axis (τ) in curved DWCNTs, e.g., the history of mass center (MC) positions of the central layer (the 41st layer) in the inner tube; the broken line (3.9273 nm) is the axial central position of the curved outer tube. (II) Rotational behavior of inner tubes in curved outer tubes, e.g., the history of the rotational frequency of the bottom layer of the inner tube. The black line indicates simulation results and the broken line is the second ordered polynomial fitting curve.

Fig 4(I) gives the history of the position of the mass center of the central layer of the inner tube. We find that stable oscillation continues for over 1600ps for straight (0°) DWCNTs, and only when the rotational speed of the inner tube becomes too low does the oscillation show disorder. In particular, during [900, 1600] ps, the oscillation is periodic, which coincides well with the conclusion given by Cai et al.¹⁵.

For 5° curved DWCNTs, stable oscillation lasts about 1200 ps from the beginning. No periodic oscillation occurs. For 15° curved DWCNTs, sub-stable oscillation occurs during [600, 2800] ps. When the angle of curvature is 25° , the oscillation of the inner tube is always chaotic. The conclusion might be drawn that stable free oscillation hardly exists in a curved DWCNT with large angle of curvature.

3.3 Rotational behavior of inner tubes in curved outer tubes

Fig 4(II) gives the damped rotation of the inner tubes in curved DWCNTs. Using the second order polynomial curve lines (the broken lines in Fig. 4(II)b) to fit the simulation results, i.e.,

$$f = A(\phi) + B(\phi) \cdot t + C(\phi) \cdot t^2 \quad (2)$$

where f is the rotational frequency of the inner tube (unit: GHz), t represents time (unit: ps), we obtain the values of the coefficients, i.e., A , B , and C , for each case (Table 2)

Table 2 The coefficients A , B , and C in Eq.(2)

Curvature	A /(GHz)	B /(GHz/ps)	C /(GHz/ps/ps)
0°	124.298	-55.119×10^{-3}	7.973×10^{-6}
5°	124.165	-56.281×10^{-3}	8.703×10^{-6}
15°	114.703	-73.802×10^{-3}	14.241×10^{-6}
25°	108.002	-87.644×10^{-3}	19.066×10^{-6}

Further, using a linear function to fit the coefficients (A , B , and C) with respect to the curvature angle, we obtain following equations:

$$\begin{aligned} A(\phi) &= 127.701 - 0.703\phi \\ B(\phi) &= -(52.652 + 1.383\phi) \times 10^{-3} \\ C(\phi) &= (7.264 + 0.465\phi) \times 10^{-6} \end{aligned} \quad (3)$$

From the above equations, coefficient A represents the initial value of rotational frequency of the inner tube; that value decreases with the increase of the curvature angle. The absolute value of coefficient B is proportional to the curvature angular value. The value of B is always negative. This means that the value of rotational frequency decreases more quickly when $t < 1000$ ps. Higher values of curvature angle lead to a greater decrease in rotational frequency.

Table 3 demonstrates that the inner tube is trapped into a curved outer tube because of the curvature of inner tube is less than that of the outer tube. Mechanically, the inner tube trends to be straight in a curved outer tube. Therefore, the distance between the two tubes is not uniform. For instance, as the difference between radii is ~ 0.335 nm, which is the equilibrium distance between two graphene sheets, the distance between the two tubes is mainly different from 0.335nm. Hence, the intertube friction is greater than that in a straight outer tube, which is the major reason for the more highly damped motion of the inner tube in a curved outer tube.

3.4 Effect of temperature on dynamics behavior of inner tubes in curved outer tubes

Here, we only study the dynamics responses of the 25° curved tubes in the canonical NVT ensemble with different temperature (100, 300 and 500 K). From Fig 5(I), we find that the inner tubes acts as an oscillator at 100 K during [2000, 2800] ps. At higher temperature (300 or 500 K), the phenomenon is not obvious. It is noted that, at higher temperature, the thermal vibration of atoms on tubes becomes drastic, which increases the friction between the two tubes. In particular, the contact area between tubes becomes coarser rather than smoother because of higher amplitude of atoms at higher temperature. Thus, the energy dissipation of the inner tube becomes faster and no enough kinetic energy to maintain the oscillation of the inner tube. From Fig 5(II), we have the

following fitting function of rotational speed (GHz) of inner tube on the temperature T (unit K).

$$\omega = A(T) + B(T) \cdot t + C(T) \cdot t^2 \quad (4)$$

with

$$\begin{aligned} A(T) &= 45.476 + 0.057T \\ B(T) &= -(27.435 + 0.104T) \\ C(T) &= 4.983 + 0.030T \end{aligned} \quad (5)$$

The time t is assumed to be in $[0, 3]$ ns. The function of “A” in Eq.(5) implies that the initial rotational speed of the inner tube decrease faster (from the input rotational speed 125 GHz) at the lower temperature. Whereas the function of “B” in Eq.(5) means that the rotational speed decreases faster at the higher temperature.

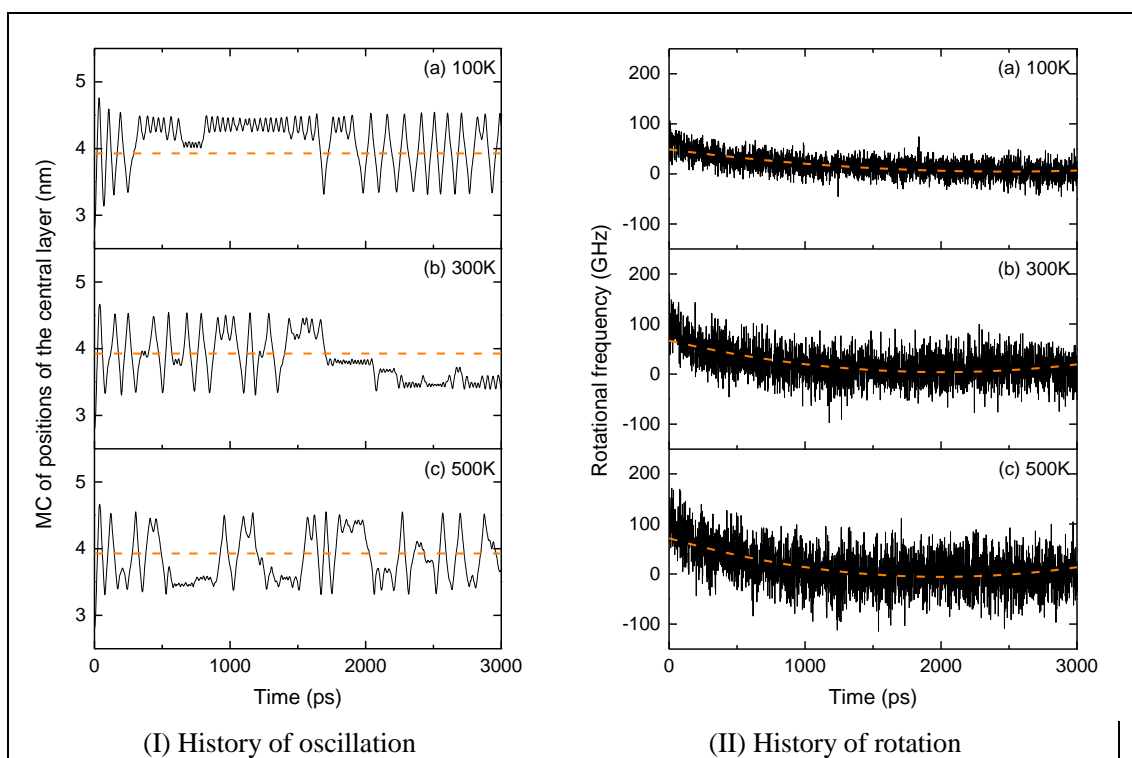


Fig 5 Damping motions of the inner tube in a NVE ensemble. (I) Oscillatory behavior of inner tube along curved axis (τ) in curved DWCNTs, e.g., the history of mass center (MC) positions of the central layer (the 41st layer) in the inner tube; the broken line (3.9273 nm) is the axial central position of the curved outer tube. (II) The history of the rotational frequency of the bottom layer of the inner tube. The broken line is the second ordered polynomial fitting curve.

Acknowledgments

Financial support from the National Natural-Science-Foundation of China (grant no. 50908190; 11372100) and the Research Foundation (grant no. GZ1205) of the State Key Laboratory of Structural Analysis for Industrial Equipment, Dalian University of Technology, China are acknowledged.

References

1. J. Servantie and P. Gaspard, *Physical review letters*, 2006, **97**, 186106.
2. Z. Qin, Q. H. Qin and X. Q. Feng, *Physics Letters A*, 2008, **372**, 6661-6666.
3. W. Qiu, Y. L. Kang, Z. K. Lei, Q. H. Qin and Q. Li, *Chinese Physics Letters*, 2009, **26**, 080701.
4. W. Qiu, Y. L. Kang, Z. K. Lei, Q. H. Qin, Q. Li and Q. Wang, *Journal of Raman Spectroscopy*, 2010, **41**, 1216-1220.
5. J. Cumings and A. Zettl, *Science*, 2000, **289**, 602-604.
6. M. F. Yu, B. I. Yakobson and R. S. Ruoff, *The Journal of Physical Chemistry B*, 2000, **104**, 8764-8767.
7. M. F. Yu, O. Lourie, M. J. Dyer, K. Moloni, T. F. Kelly and R. S. Ruoff, *Science*, 2000, **287**, 637-640.
8. Q. S. Zheng and Q. Jiang, *Physical Review Letters*, 2002, **88**, 045503.
9. Q. S. Zheng, J. Z. Liu and Q. Jiang, *Physical Review B*, 2002, **65**, 245409.
10. S. B. Legoas, V. R. Coluci, S. F. Braga, P. Z. Coura, S. O. Dantas and D. S. Galvão, *Physical Review Letters*, 2003, **90**, 055504.
11. Y. Zhao, C. C. Ma, G. H. Chen and Q. Jiang, *Physical Review Letters*, 2003, **91**, 175504.
12. J. L. Rivera, C. McCabe and P. T. Cummings, *Nanotechnology*, 2005, **16**, 186-198.
13. J. L. Rivera, C. McCabe and P. T. Cummings, *Nano Letters*, 2003, **3**, 1001-1005.
14. W. Guo, Y. Guo, H. Gao, Q. Zheng and W. Zhong, *Physical Review Letters*, 2003, **91**, 125501.
15. K. Cai, H. Yin, Q. H. Qin and Y. Li, *Nano letters*, 2014, **14**, 2558-2562.
16. A. Neild, T. W. Ng and Q. Zheng, *Epl*, 2009, **87**, 16002.
17. J. W. Kang, K. Kim, H. J. Hwang and O. K. Kwon, *Physics Letters A*, 2010, **374**, 3658-3665.
18. H. Ustunel, D. Roundy and T. A. Arias, *Nano Letters*, 2005, **5**, 523-526.
19. F. N. Mayoof and M. A. Hawwa, *Chaos Solitons & Fractals*, 2009, **42**, 1860-1867.
20. W. Xia and L. Wang, *Computational Materials Science*, 2010, **49**, 99-103.
21. H. M. Ouakad and M. I. Younis, *Journal of Sound and Vibration*, 2011, **330**, 3182-3195.
22. E. Ghavanloo, M. Rafiei and F. Daneshmand, *Physics Letters A*, 2011, **375**, 1994-1999.
23. R. Artan and A. Tepe, *Mechanics of Advanced Materials and Structures*, 2011, **18**, 347-351.
24. A. Eichler, J. Moser, M. I. Dykman and A. Bachtold, *Nature Communications*, 2013, **4**, 2843.
25. M. M. S. Fakhrabadi, P. K. Khorasani, A. Rastgoo and M. T. Ahmadian, *Solid State Communications*, 2013, **157**, 38-44.
26. S. J. Stuart, A. B. Tutein and J. A. Harrison, *Journal of Chemical Physics*, 2000, **112**, 6472-6486.
27. K. Cai, J. Yu, H. Yin and Q. Qin, *Nanotechnology*, 2015, **26**, 095702.